A search for transient reductions in the inflaton speed of sound in cosmological data, and other topics

Torrado Cacho, J.

Author: Torrado Cacho, Jesús
Title: A search for transient reductions in the speed of sound of the inflaton in cosmological data, and other topics
Issue Date: 2015-03-31

Chapter 2

Localized correlated features in the CMB power spectrum and primordial bispectrum from a transient reduction in the speed of sound

Foreword

This chapter is based on the published papers

> **Localized correlated features in the CMB power spectrum and primordial bispectrum from a transient reduction in the speed of sound**
>
> Ana Achúcarro, Vicente Atal, Pablo Ortiz, and Jesús Torrado
>
> Published in Physical Review D89 (2014) 103006
>
> Preprint in arXiv:1311.2552 [astro-ph.CO]

and

> **Inflation with moderately sharp features in the speed of sound: GSR and in-in formalism for power spectrum and bispectrum**
>
> Ana Achúcarro, Vicente Atal, Bin Hu, Pablo Ortiz, and Jesús Torrado
>
> Published in Physical Review D90 (2014) 023511
>
> Preprint in arXiv:1404.7522 [astro-ph.CO]

The results presented in them and reproduced here are the product of the combined effort of all its authors, who, as is customary in Theoretical Cosmology, appear in alphabetical order.

As part of this Ph.D. thesis, I reproduce a major part both of the original publications, focusing on the parts in which my contribution was most significant, specially the sections concerning the parameter estimation and the interpretation of the results.

Abstract

We perform a search for localized oscillatory features in the Planck CMB power spectrum of the first year of observations, assuming that said features are caused by a transient reduction in the speed of sound of the adiabatic mode during effectively single-field, uninterrupted slow-roll inflation.

We find several fits, in which we perform several consistency checks and further analyses, such as its reproduction by the a different Boltzmann code, the study of their polarization signal in the CMB and their local significance at different angular scales.

For each of the best fits, we calculate the expected correlated signal in the primordial bispectrum, and compare it to the search for scale dependent bispectrum features carried out by the Planck collaboration. Where both searches overlap, we reproduce the Planck results reasonably well. In addition, some of our best fits lie outside the scales and frequency ranges searched by Planck, which calls for an extension in frequencies and envelopes of the templates used in Planck's search.

By exploiting correlations between different observables, our results strongly suggest that current and data, including the imminent 2014 Data Release of Planck, might already be sensitive enough to detect transient reductions in the speed of sound as mild as a few percent, opening a new window for the presence of extra degrees of freedom during inflation.

2.1 Introduction

The paradigm of inflation [47, 71, 72, 70, 55, 18] in its simplest realizations is consistent with the latest data releases from the Planck [7] and WMAP [28] satellites. However, hints of a primordial oscillatory signal in the CMB bispectrum [10] and of anomalies in the CMB power spectrum [28, 9] motivate a search for correlated features produced by inflationary scenarios beyond canonical single-field.[1] Such correlation is in general expected and will differ depending on its physical origin [34], so it can be used to discriminate among inflationary mechanisms.

On the theory side, several mechanisms that produce oscillatory features are being investigated. As first noted in [73], a step in the inflaton potential causes

[1] By canonical single-field we mean slow-roll regime, Bunch-Davies vacuum, canonical kinetic terms and minimal coupling to gravity, with speed of sound $c_s = 1$.

features in the spectra [77, 6, 45, 21, 33, 19, 57, 12, 20, 75, 23], and novel methodologies have been developed in [74, 35, 38, 15, 63, 16] for more generic transient slow-roll violations. The effect of a variable speed of sound has also been analysed both in the power spectrum [2, 50, 5] (for sudden variations see [66, 63, 64, 24, 23]) and bispectrum [5, 16, 68] (see [24, 23] for sudden variations). Different initial vacuum states (see e.g. [37, 46, 61, 51]) or multi-field dynamics [44, 43, 69, 65] may also cause oscillations in the primordial spectra.

On the observational side, searches in the CMB power spectrum data have been performed for a variety of scenarios, such as transient slow-roll violations [36, 12, 26, 13, 25, 48, 27, 63], superimposed oscillations in the primordial power spectrum [56, 42, 17, 58, 67, 60, 59] and more general parametric forms (see [9] and references therein). In addition, the Planck collaboration searched for features in the CMB bispectrum for a number of theoretically motivated templates [10]. In none of these cases the statistical significance of the extended models has been found high enough to claim a detection. Still, it is becoming clear that hints of new physics (if any) are most likely to be detected in the correlation between different observables.

In this spirit, in the two papers presented in this chapter we search for transient reductions in the speed of sound of the adiabatic mode consistent with (effectively) single-field inflation and *uninterrupted* slow-roll. We do this by exploiting a very simple correlation between power spectrum and bispectrum noted in [5] and presented in section 1.3.4. While more general situations are possible, and have been considered elsewhere [15, 16], there is a particularly interesting regime for which the *complete* primordial bispectrum is obtained to leading order in slow-roll [5]. The amplitude and the rate of change of the speed of sound must be large enough to dominate over slow-roll effects while being small enough to allow a perturbative calculation of the effect on the power spectrum and bispectrum. We call transient reductions in this regime *mild and moderately sharp*.

Our test case consists of a gaussian reduction in the speed of sound occurring within the window of e-folds in which the scales corresponding to the angular scales probed by Planck exit the Hubble sound horizon. The functional form is inspired by soft turns along a multi-field inflationary trajectory with a large hierarchy of masses, a situation that is consistently described by an effective single-field theory [3, 2, 31, 4] (see also [44, 43]). Nevertheless we stress that reductions in the speed of sound are a more general phenomenon within effective field theory (and hence may have diverse physical origins).

Our statistical analysis of the Planck CMB power spectrum reveals several fits with a moderately improved likelihood compared to the best ΛCDM fit. We performed different tests to check the robustness of the fits found. For each of those fits we give the associated full primordial bispectrum. At the time of writing this thesis, the Planck bispectrum data have not yet been released but, due to a lucky coincidence, templates very similar to our predictions have already been tested by Planck [10] (inspired by a step in the potential). We find that the predicted bispectra for some of our fits are reasonably consistent with the best fits of Planck. In addition, some of our best fits lie on a region of the parameter space not yet analysed by Planck. If confirmed, these correlations would constitute evidence for transient reductions in the speed of sound. It is interesting that rather mild reductions of the order of a few percent may already be observable in the data.

2.2 Our test case – A gaussian in *e*-folds

In this chapter, we attempt to fit to the CMB data the kind of features described in section 1.3.4. The features in the CMB temperature power spectrum originate from the perturbations in the scalar primordial power spectrum given by eq. (1.54), in terms of a reduction in the speed of sound $c_s(\tau)$.

We have chosen to parametrise the reduction in the speed of sound as a *gaussian* in e-folds N. This functional form is inspired by soft turns along a multi-field inflationary trajectory with a large hierarchy of masses, a situation that is consistently described by an effective single-field theory and uninterrupted slow roll [3, 2, 31, 4, 44, 43]. Our parametrisation reads:

$$u = 1 - c_s^{-2} = B\, e^{-\beta(N-N_0)^2} = B\, e^{-\beta\left(\ln \frac{\tau}{\tau_0}\right)^2}\ , \tag{2.1}$$

where $\beta > 0$ is the sharpness, $B < 0$ is the amplitude, and N_0 (or τ_0) is the instant of maximal reduction. Assuming slow-roll, the conformal time τ is related to the e-folds of inflation through $\ln(-\tau) = (N_{\rm in} - N) - \ln(a_{\rm in} H_0)$, where $a_{\rm in} = a(N_{\rm in})$ and $N_{\rm in}$ is the time when the last ~ 60 e-folds of inflation start. Notice that the quantity $N_{\rm in}$ is irrelevant, since all the quantities in e-folds are defined with respect to $N_{\rm in}$.

There are two main criteria that we followed in order to determine the parameter regions that we would explore:

(a) The SRFT calculation of the power spectrum and the bispectrum is valid for *mild and moderately sharp* reductions of the speed of sound. Also, the slow-roll contributions to the bispectrum are disregarded with respect to the terms arising from the reduced speed of sound (see [5] or section 1.3.4). This means that the amplitude $|u|$ and the rate of change $s \equiv \frac{\dot{c}_s}{c_s H}$ must be much smaller than one, while being (at least one of them) much larger than the slow-roll parameters. The rate of change s of the speed of sound (2.1) reads:

$$s(N) = \frac{dc_s}{c_s dN} = -\frac{B\beta(N-N_0)\, e^{-\beta(N-N_0)^2}}{1 - B\, e^{-\beta(N-N_0)^2}}\ . \tag{2.2}$$

Since we have to impose $|s| \ll 1$ for all values of N, it suffices to impose this condition at the point where $|s|$ takes its maximum value $|s(N_*)| = |s|_{\max}$, determined by

$$N_* = N_0 \pm \frac{1}{\sqrt{2\beta}}\sqrt{1+\mathcal{O}(B)} \;\simeq\; N_0 \pm \frac{1}{\sqrt{2\beta}}\ , \tag{2.3}$$

which approximately corresponds to one standard deviation of our gaussian, and we have used that $|B| \ll 1$. Then the condition $|s|_{\max} \ll 1$ translates into $\beta \ll \frac{2e}{B^2} + \mathcal{O}(B^{-1})$. Altogether, the allowed region of our parameter space taking into account these constraints is

$$\mathcal{O}(\epsilon,\eta) \ll |B| \ll 1\ , \tag{2.4a}$$

$$\beta_{\min} \ll \beta \ll \frac{2e}{B^2}\ , \tag{2.4b}$$

$$N_{\rm bb} < N_0 < N_{\rm end}\ , \tag{2.4c}$$

where $N_{\rm bb}$ and $N_{\rm end}$ are respectively the (unknown) instants, in e-folds scale, of the beginning and the end of inflation; on the other hand, $\beta_{\min}$ corresponds to the case in which $|s|_{\max} \sim \mathcal{O}(\epsilon,\eta)$. Notice that it is only necessary to satisfy one of the lower limits of eqs. (2.4a) or (2.4b).

(b) The angular scales probed by Planck ($\ell = 2 - 2500$) roughly correspond to the momentum scales crossing the Hubble sound horizon during the first $N_{\rm CMB} \simeq 7$ e-folds of the last ~ 60 e-folds of inflation. If the data resembles features due to a reduced speed of sound, it is most likely to find them within this *CMB window* (we choose to *look under the lamppost*). This translates into constraints on the parameters that determine the position and width of the feature, namely the sharpness β and the instant N_0. They are chosen so that the reduction happens well within this CMB window. We took a very conservative definition for the total width of the reduction (in e-folds): ten standard deviations of the gaussian, $\Delta N = 10/\sqrt{2\beta}$, must fit within the observable window $[N_{\rm in},\, N_{\rm in} + N_{\rm CMB}]$. Then, the position N_0 and the sharpness β should satisfy

$$\frac{50}{N_{\rm CMB}^2} < \beta\ , \tag{2.5a}$$

$$\frac{5}{\sqrt{2\beta}} < N_0 - N_{\rm in} < N_{\rm CMB} - \frac{5}{\sqrt{2\beta}}\ . \tag{2.5b}$$

This is a very conservative choice (or, the *lamppost* reaches actually further): (2.5a) and (2.5b) are more restrictive than the condition that the feature be observable: for example, any feature happening in a particular window has an effect on the modes that leave the horizon after the reduction in c_s has finished, as is shown by the fact that the transfer functions that relate primordial scales when they leave the Hubble sphere to scales in the CMB have a non-zero, finite width. In exchange for a more restrictive constraint, we avoid degeneracies with the spectral index n_s and the optical depth $\tau_{\rm reio}$ that could be caused by reductions with a very long wavelength in the power spectrum.

Finally, putting together the constraints described above, and prioritising the most restrictive of them in each case, we get the final set of bounds

$$\mathcal{O}(\epsilon,\eta) \ll |B| \ll 1 \ , \tag{2.6a}$$

$$\frac{50}{N_{\rm CMB}^2} < \beta \ll \frac{2e}{B^2} \ , \tag{2.6b}$$

$$\frac{5}{\sqrt{2\beta}} < N_0 - N_{\rm in} < N_{\rm CMB} - \frac{5}{\sqrt{2\beta}} \ . \tag{2.6c}$$

For computational purposes, we use the parameter $\ln(-\tau_0)$ instead of N_0 for the data analysis. The range for this parameter is taken to be more strongly restricted than by (2.6c):

$$4.4 \leq \ln(-\tau_0) \leq 6 \ . \tag{2.7}$$

The features in the power spectrum and bispectrum are linearly oscillating, as well as those tested in one of the searches for bispectrum features by the Planck collaboration [10, sec. 7.3.3]. The oscillatory frequency is determined by τ_0, and the range of frequencies covered in Planck's bispectrum analysis is equivalent to the interval $\ln(-\tau_0) \in [4.43, 5.34]$. This motivates us to search in the interval given above, which contains and slightly enlarges that of Planck's search, while as the same time avoids highly oscillating features (larger values of $|\tau_0|$) that make computational control difficult.

As a final step, we choose priors for the three parameters of the feature. In particular, we choose uniform priors in B, $\ln\beta$ and $\ln(-\tau_0)$, within the limits given respectively by eqs. (2.6a), (2.6b) and (2.7). The model-dependent bound $|B| \gg \mathcal{O}(\epsilon,\eta)$ is ignored a priori.

2.3 Methodology of the search

The power spectrum features caused by a transient reduction in the speed of sound described by eq. (2.1), are combined with the primordial spectrum of the ΛCDM Planck baseline model described in [11, sec. 2], parametrized by an amplitude A_s and a spectral index n_s. To do so, we solve the integral in eq. (1.54) using a Fast Fourier Transform. The primordial perturbations evolve in a flat FLRW universe parametrized by the densities of baryonic and cold dark matter, $\Omega_{\rm b}$ and $\Omega_{\rm cdm}$, and the current expansion rate H_0. The damping due to reionisation is parametrized by the optical depth $\tau_{\rm reio}$. Those 6 standard plus 3 feature parameters describe our cosmological model.

The evolution of the perturbations and their projection onto the CMB power spectrum is calculated with the Boltzmann code CLASS [52, 29]. In order to incorporate our features to the primordial power spectrum, we needed to develop an extension to CLASS, which is described in chapter 4.

The resulting CMB is fitted to the ESA Planck mission temperature data of March 2013, using the likelihood provided by the experiment [8], and the low-ℓ CMB polarization data of the WMAP experiment [28]. We use flat priors on the 6 ΛCDM parameters and the 14 nuisance parameters of the likelihood [8]. For the parameters of the feature, we use the priors described in the last section. The posterior probability is then maximized over the prior bounds using Markov-Chain Monte-Carlo (MCMC) methods, making use of the MCMC sampler Monte Python [22].

Multi-modal sampling with Markov Chain Monte Carlo

As is usual when fitting small features on top of a large data set, we found the likelihood pdf (and hence the posterior) to be multi-modal. Although multi-modal distributions are sampled more efficiently with methods such as *multi-modal nested sampling* [41, 40], we managed to sample the posterior pdf by using only MCMC methods. As we explained in section 1.5.7, the reason why MCMC methods fall short when exploring multi-modal pdf's is the need for a very long sampling time in order for the jumping between different modes to occur enough to, at the same time, (1) sampling each of the modes fairly with respect to each other, and (2) finely sampling around each one of them. It is easy to show why it is difficult to have both: finely sampling around each of the modes requires a proposal distribution as close as possible to that of the mode itself, which automatically sets the step size in the parameter space to be much smaller than the distance between well-separated modes, making jumps between them unlikely; on the other hand, an extended proposal distribution characterises better the position of the different modes, but sets the step-size so large that the estimation of the confidence intervals of each of the modes is quite inaccurate, since the sampling around each of the maxima is scarce.

In this work, instead of finding a compromise solution, we took a two-steps approach. First, we sampled the posterior pdf with an extended proposal distribution, in order to find the rough position and shape of the different modes, but renouncing to get accurate parameter constrains for now.[2] After obtaining a big number of samples, we inspected the resulting *profile* of the posterior pdf in a grid – the profile pdf $\mathcal{P}(\alpha_i)$ in a grid cell i with respect to a subset of the full set of parameters $\{\alpha\} \subset \{\theta\}$ is the maximised pdf with respect to the remaining parameters and the cell volume, $\mathcal{P}(\alpha_i) = \max_{\{\theta\}-\{\alpha\},i}\mathcal{P}(\theta)$. Why the profile and not, as it is usual, the marginal pdf? Because the large extent of the proposal

[2] It is common in MCMC samplers, when there is no good estimate of the proposal distribution, to start the sampling process with an inaccurate estimate, and then use some of the first samples to obtain a more accurate one and to automatically restart the sampling with this one. Needless to say, in this setting this approach is not appropriate, since we do prefer a rough, long-tailed, inaccurate proposal pdf to be constant during the whole sampling process.

distribution produces a very scarce sampling that makes the different modes only barely visible as over-densities of samples (as local maxima of the marginal likelihood); instead, they are easier to see by directly inspecting the values of the likelihood on a coarse grid.

Second, once the rough shape of the pdf is known, provided that the different modes are clearly separated, one can crop regions of the parameter space containing each a single mode. Over each of those regions, using a rough estimate of the single-mode proposal distribution, one can obtain confidence intervals for the different parameters as one would normally do for uni-modal pdf's. Finally, each of the modes must be assigned a relative probability proportional to the total pdf mass under said mode.

Going back to the particular case under study, as our features are small and affect only a fraction of the data set, we expect to find only mild degeneracies of the feature parameters with the cosmological parameters. Due to the mild character of the degeneracies (that we confirmed a posteriori, cf. fig. 2.2), we expect the likelihood to show its multi-modal character only within the parameter subspace of the feature. Therefore, we started our search by mapping the multi-modal likelihood on this 3-dimensional subspace.

We started our analysis by sampling the parameter sub-space of the feature, $(B,\, \ln\beta,\, \ln(-\tau_0))$, with very long tailed chains, of order 5% of the width of the prior in each direction. After obtaining a big number of samples, we inspected the profile posterior in the plane $(\ln\beta,\, \ln(-\tau_0))$; it revealed the position and rough size of the different modes, and we used that information to crop uni-modal regions. We then reassessed the shape of the modes by sampling over the feature parameters only, and when their position and extension were sufficiently well determined, we resampled them allowing now the baseline ΛCDM and nuisance parameters to vary. With this, we got the definitive posterior probability distribution functions for the different modes.

In the following, χ^2 refers to the so-called *effective* χ^2 defined as $\chi^2_{\rm eff} = -2\ln\mathcal{L}$ (see [76, p. 10]); in turn, $\Delta\chi^2$ stands for the difference with the corresponding best fit value of Planck baseline model, using the likelihoods mentioned above [11]: $\chi^2_{\text{eff, best-fit}} = 9805.90$.

2.4 Summary and analysis of the results

The result of our search, having discarded small signals with $\Delta\chi^2 > -2$ over ΛCDM, is a series of five well-isolated bands with almost constant $\ln(-\tau_0)$ (i.e. frequency of oscillation of the feature in the primordial spectrum), in which the likelihood is *improved* with variable significance. We will call them, in order of decreasing $\ln(-\tau_0)$, *modes* $\mathcal{A}$ to $\mathcal{E}$. The resulting profile likelihood can be seen in figure 2.1. For each of the modes showed in the figure, the relevant parameter data is given in table 2.1: the numbers in parentheses are the best fit values, and

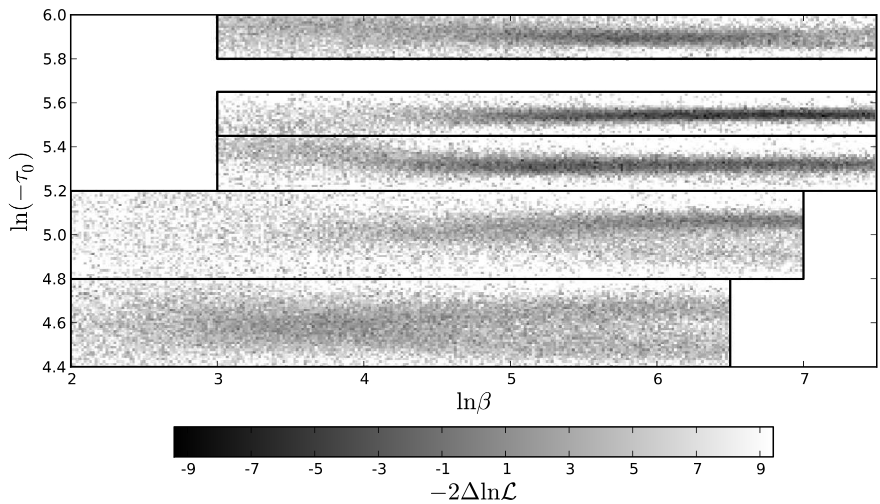

Figure 2.1: Profile of $\Delta\chi^2 = -2\Delta\ln\mathcal{L}$ for the features in the CMB power spectrum in the $(\ln\beta,\, \ln(-\tau_0))$ plane. We name each of the bands, in descending order of $\ln(-\tau_0)$, *modes* $\mathcal{A}$ to $\mathcal{E}$. Regions with improvements of $-\Delta\chi^2 < 2$ have been discarded and are not shown in the plot.

Mode	$-B \times 10^2$	$\ln\beta$	$\ln(-\tau_0)$	$\Delta\chi^2$	$s_{\max}$
$\mathcal{A}$	$(4.5)\, 3.7\,^{+1.6}_{-3.0}$	$(5.7)\, 5.7\,^{+0.9}_{-1.0}$	$(5.895)\, 5.910\,^{+0.027}_{-0.035}$	-4.3	0.33
$\mathcal{B}$	$(4.2)\, 4.3 \pm 2.0$	$(6.3)\, 6.3\,^{+1.2}_{-0.4}$	$(5.547)\, 5.550\,^{+0.016}_{-0.015}$	-8.3	0.42
$\mathcal{C}$	$(3.6)\, 3.1\,^{+1.6}_{-1.9}$	$(6.5)\, 5.6\,^{+1.9}_{-0.7}$	$(5.331)\, 5.327\,^{+0.026}_{-0.034}$	-6.2	0.40
$\mathcal{D}$	(4.4)	(6.5)	(5.06)	-3.3	0.48
$\mathcal{E}$ *	(1.5)	(4.0)	(4.61)	-2.2	0.05

Table 2.1: CMB power spectrum best fits (in parentheses), 68% c.l. intervals, effective $\Delta\chi^2$ at the best fit value, and maximum value of the speed of sound derivative $s_{\max}$, for each of the modes. The prediction for the bispectrum for $\mathcal{E}$ is not reliable (see text).

the parameter ranges, when given, are 68% c.l. regions.

The amplitude B of the fits is rather small, $\mathcal{O}(10^{-2})$, and therefore comparable with neglected slow-roll terms. This means the bispectrum is dominated by terms of order $s = \dot{c_s}/(Hc_s)$. The maximum values of s at the best fits for the modes $\mathcal{A}$ to $\mathcal{E}$ in table 2.1 are respectively 0.33, 0.42, 0.40, 0.48, 0.05. Notice that the value of s for $\mathcal{E}$ is also comparable to neglected terms, so the prediction for the bispectrum based on eq. (1.55) cannot be trusted in this case. We therefore disregard this mode in the comparison with the bispectrum.

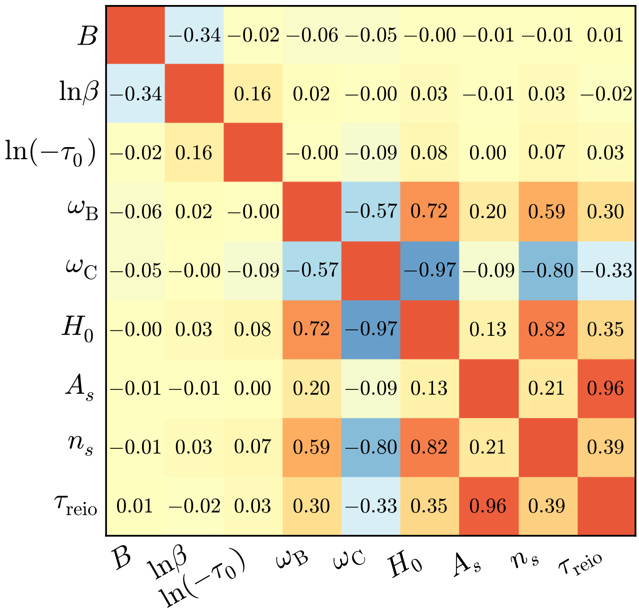

Figure 2.2: Correlation coefficients between the feature and the cosmological parameters for the mode $\mathcal{B}$. Notice the small correlations between the two sets of parameters, and the rather large negative correlation between B and $\ln\beta$.

For the modes $\mathcal{A}$, $\mathcal{B}$ and $\mathcal{C}$ the table 2.1 shows the 68% c.l. ranges. For bands $\mathcal{B}$ and $\mathcal{C}$ we were unable to put an upper bound on $\ln\beta$ due to a degeneracy between that parameter and the amplitude $|B|$, as we will explain below. For those two modes, the upper bound on $\ln\beta$ is set by the prior $s < 1$ in eq. (2.6b), which is saturated at $\ln\beta \simeq 7.5$.

The lower bands $\mathcal{D}$ (and $\mathcal{E}$) are less significant and their likelihoods much less gaussian, so we only show their best fits. Despite their low significance, they are worthy of mention because they fall in the region overlapping with Planck's search for features in the bispectrum (see below).

The best fits and 68% c.l. ranges of the six ΛCDM parameters [11][3] are quite accurately reproduced, see table 2.2. As expected, we find only small degeneracies[4] ($|\rho| \leq 0.15$) between the feature parameters and the ΛCDM parameters for modes $\mathcal{A}$, $\mathcal{B}$ and $\mathcal{C}$. The correlation matrix for the mode $\mathcal{B}$ is shown in fig. 2.2. For the less significant modes $\mathcal{D}$ and $\mathcal{E}$, some of the correlations grow up to $|\rho| \leq 0.30$.

[3] See also the parameter tables at `http://www.sciops.esa.int/wikiSI/planckpla/index.php?title=File:Grid_limit68.pdf&instance=Planck_Public_PLA`.

[4] The correlation matrix is defined as $\rho_{ij} \equiv C_{ij}/\sqrt{C_{ii} \cdot C_{jj}}$, where C_{ij} are the covariance matrix elements corresponding to the parameters with indices i and j.

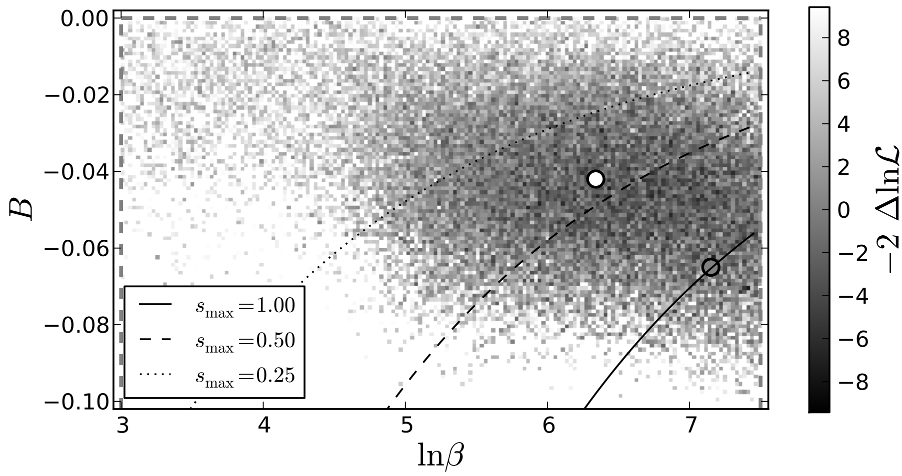

Figure 2.3: Profile of $\Delta\chi^2 = -2\Delta\ln\mathcal{L}$ for the mode $\mathcal{B}$ in the $(\ln\beta,\, B)$ plane, showing the $\rho = -0.34$ degeneracy between those two parameters. Some lines of $s_{\max}$ = const are shown. Notice how the mode extends beyond the $s = 1$ prior limit.

This is expected, since for lower $\ln(-\tau_0)$ the frequency of the fits drops, getting closer to the frequency of the acoustic oscillations.

A gain of $|\Delta\chi^2| \lesssim 10$ is common in similar searches (see section 2.4.4 for a comparison with other searches for features in the CMB power spectrum), which suggests that CMB power spectrum data alone cannot justify the introduction of these features. Nevertheless, the aim of this chapter is to show that low-significance fits can still predict correlated features in the bispectrum which are possibly observable with the current data. Model selection should be done using the full parameter ranges allowed by the theory and taking into account both power spectrum and bispectrum, and, if possible, adding other data sets with uncorrelated systematic effects, such as Large Scale Structure (see chapter 3).

2.4.1 The degeneracy of B and $\ln\beta$ – upper limit of $\ln\beta$

In this section we comment on one characteristic of the modes $\mathcal{B}$ and $\mathcal{C}$ (and also $\mathcal{D}$): a positive correlation between $\ln\beta$ and $|B|$: the CMB temperature data is not able to restrict the maximum value of $\ln\beta$, as one can see in figure 2.1 and in the 1D marginalized likelihood of $\ln\beta$ in figure 2.6 (middle-right panel). In each mode, after some value of $\ln\beta$, the likelihood reaches a plateau with constant $\ln(-\tau_0)$; along this direction of increasing $\ln\beta$, the best-fit amplitude B grows (see fig. 2.3), correlated with $\ln\beta$ with correlation coefficient of order $\rho \sim -0.3$ (cf. fig. 2.2). The simultaneous growth of $|B|$ and $\ln\beta$ in some of these plateaus causes that at some point the prior limit $s < 1$ in eq. (2.6b) gets saturated, in particular at $\ln \beta \simeq 7.5$ (see figure 2.3), and hence the prior sets the upper bound for $\ln \beta$.

From the CMB power spectrum point of view, the reason for this to happen is the following: along the direction of simultaneous increase of $\ln \beta$ and $|B|$, the feature in the *primordial* power spectrum broadens towards smaller scales, while the amplitude of the tail on the larger scales remains almost constant (see 2.4, top). Since at smaller scales much of the primordial signal is suppressed by diffusion damping in the CMB, no significance is gained along the degeneracy direction, causing a plateau in $\Delta\chi^2$. This can be seen illustrated for mode $\mathcal{B}$ in figure 2.4: we compare two of the best fits of this mode, one sitting well within the prior bounds (white circle in figure 2.3), and a similar fit (grey circle in figure 2.3) that improves $\Delta\chi^2$ marginally and saturates the $s = 1$ bound. In figure 2.4 we can see the effect of those fits in the primordial and CMB temperature power spectrum. Notice how the big difference between both fits in the former gets diluted in the latter.

Can we resolve this ambiguity? Probably: photon diffusion at the last scattering surface has the effect of polarizing the CMB signal through Thomson scattering, so at smaller scales the polarization spectrum will contain information about the primordial spectrum, complementary to that of the temperature spectrum. Therefore, the difference at small scales between two fits in the same plateau (here, the dashed and dotted spectra in figure 2.4) is larger in the TE and EE CMB polarization spectra (see fig. 2.5). This suggests that the high-ℓ Planck polarization data, expected to be released along 2014, may be able to set stringer bounds on the maximum value of $\ln \beta$, as well as confirm that we are not fitting noise.

2.4.2 Cross-check with a different Boltzmann code

In order to make our results from CLASS+Monte Python more reliable, we cross-checked them with an independent Einstein-Boltzmann solver and a different MCMC sampler, namely CAMB [54] and CosmoMC [53]. As an example, in fig. 2.6 and tab. 2.2 we explicitly show this comparison for the most significant mode $\mathcal{B}$ by varying both the primary ΛCDM parameters and the additional sound speed reduction parameters. We find excellent agreement between these two results.

2.4.3 Local improvement at different angular scales: $\Delta\chi^2(\ell)$

Given a fit to the CMB power spectrum of some feature model, it is interesting to know in which ranges of multipoles the feature describes the data better than the baseline ΛCDM model. This kind of *local improvement* can only be calculated approximately, since the temperature data points at different multipoles are in general correlated. Nevertheless, even a qualitative analysis can shed some light on where the feature fits better the data than the baseline model.

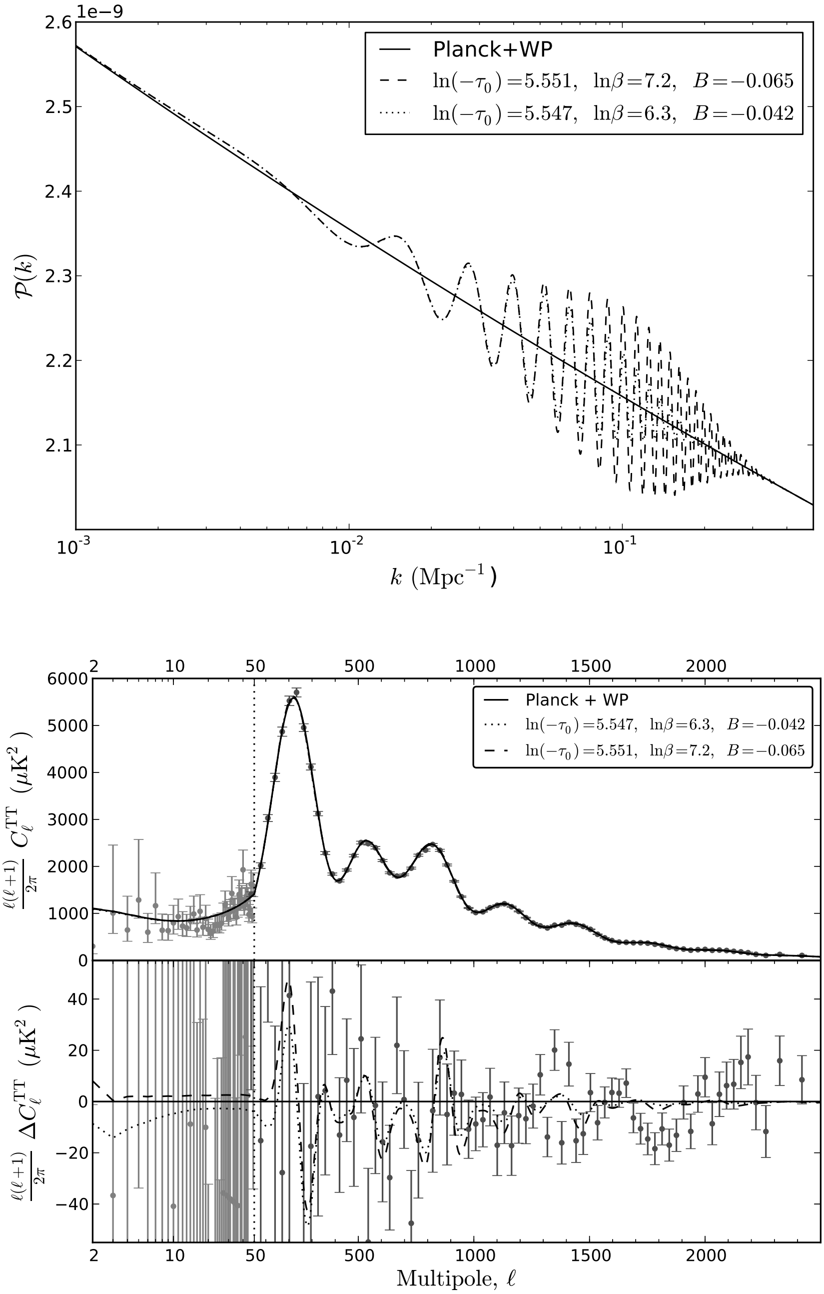

Figure 2.4: Comparison of the two fits indicated in figure 2.3 with a white circle (dotted line) and a grey circle (dashed line), in the primordial power spectrum and the TT CMB power spectrum.

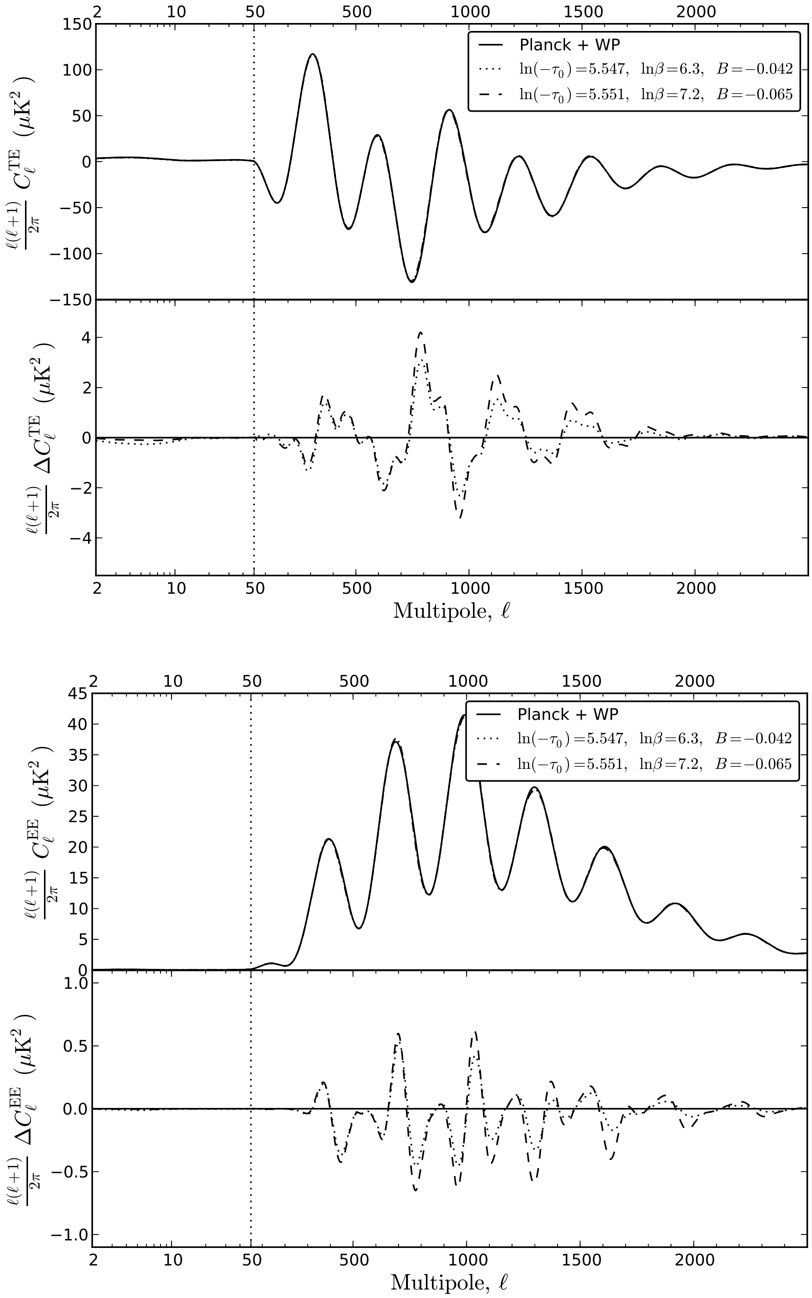

Figure 2.5: Comparison of the two fits indicated in figure 2.3 with a white circle (dotted line) and a grey circle (dashed line), in the TE and EE CMB power spectra.

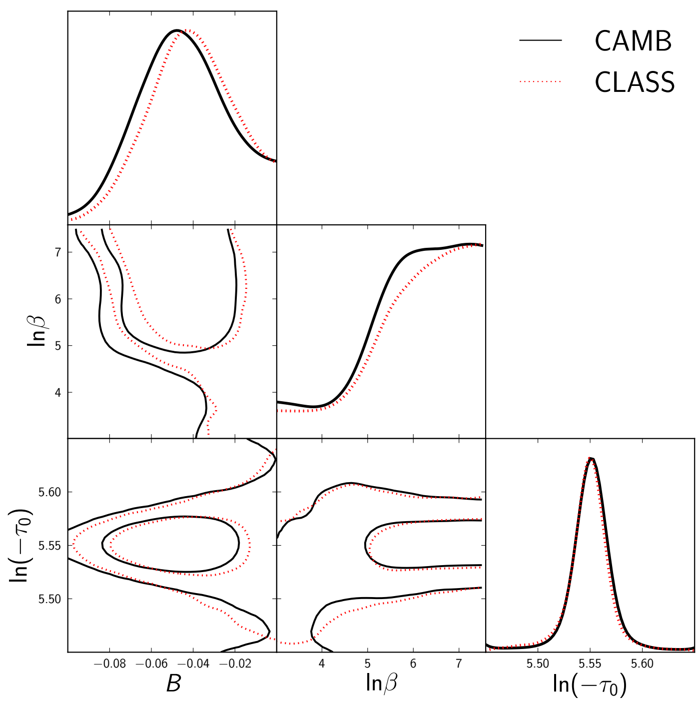

Figure 2.6: CAMB+CosmoMC vs. CLASS+Monte Python consistency check: 1D and 2D marginalized posterior distributions of the sound speed reduction parameters for the mode $\mathcal{B}$.

We have studied the local improvements along the multipoles of the four relevant fits, modes $\mathcal{A}$ to $\mathcal{D}$ (we show the result for mode $\mathcal{B}$ in figure 2.7). To do that, we have binned the multipoles with $\Delta\ell = 20$ and substituted pieces of the best fit for each mode into the best fit of the ΛCDM baseline model. For the sake of simplicity, we use for this analysis the preliminary fits found by keeping the cosmological and nuisance parameters fixed to their best fit values (hence the small difference in the total $\Delta\chi^2$ between fig. 2.7 and tab. 2.1).

The results show that mode $\mathcal{A}$ gains its significance mostly in the first and third peak and loses some of it in the second; mode $\mathcal{B}$ (see fig. 2.7) and $\mathcal{C}$ gain most of their significance in the third peak, lose some of it in the fourth peak and improve a little again in the fifth and sixth. The mode $\mathcal{D}$ does not fit well the first and second peaks, gains most of its significance in the third peak, and some more in the fifth and sixth peaks.

***Planck*+WP**			
Parameter	CAMB	CLASS	Baseline [11]
$100\Omega_b h^2$	2.208 ± 0.027	2.214 ± 0.029	2.205 ± 0.028
$\Omega_c h^2$	0.1204 ± 0.0026	0.1203 ± 0.0027	0.1199 ± 0.0027
$\tau_{\rm reio}$	0.089 ± 0.013	0.090 ± 0.013	$0.089^{+0.012}_{-0.014}$
H_0	67.16 ± 1.14	67.29 ± 1.21	67.3 ± 1.2
n_s	0.9600 ± 0.0070	0.9598 ± 0.0074	0.9603 ± 0.0073
$\ln(10^{10} A_s)$	3.090 ± 0.023	3.088 ± 0.024	$3.089^{+0.024}_{-0.027}$
B	$-0.045^{+0.045}_{-0.034}$ (95%c.l.)	$-0.041^{+0.041}_{-0.031}$ (95%c.l.)	—
$\ln \beta$	$6.00^{+1.50}_{-3.00}$ (95%c.l.)	$6.06^{+1.44}_{-2.18}$ (95%c.l.)	—
$\ln(-\tau_0)$	5.55 ± 0.06 (95%c.l.)	5.55 ± 0.05 (95%c.l.)	—
$\chi^2_{\rm bf}$	9797.25	9797.58	9805.90

Table 2.2: CAMB+CosmoMC vs. CLASS+Monte Python consistency check: mean values and 68% (or 95% where indicated) confidence intervals for the primary ΛCDM parameters and the additional sound speed reduction parameters for the mode $\mathcal{B}$. We also show the parameter ranges found by the Planck collaboration [11] for a featureless model.

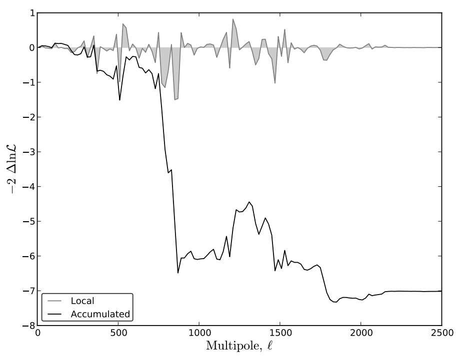

Figure 2.7: Local gain in the likelihood of the best fit of mode $\mathcal{B}$ along the multipoles. The grey area shows the local difference in each bin, and the black line shows the accumulated difference for increasing multipoles.

2.4.4 Comparison with other searches for features in the CMB power spectrum

Due to the Fourier transform in eq. (1.54), our features oscillate as $\exp(i2k\tau_0)$. Thus it is natural to compare to other searches for linearly oscillating features in the Planck CMB power spectrum.

Ref. [59] searches for non-localized features with frequencies that compare to ours as $\omega_2 = 2|\tau_0|$. In the overlapping region, $\omega_2 \in [160, 810]$, they find peaks at roughly $\ln(-\tau_0) \sim \{5.0, 5.1, 5.3, 5.6, 5.7\}$ ($|\Delta\chi^2_{\rm bf}| \simeq 8$). We find three peaks in this region with similar significance; it could be that the discrepancies come from signals at scales at which our (localized) features are negligible.

Also, the Planck collaboration [9, sec. 8] searches for features motivated by step-inflation, using the parametrization proposed in [13] with a frequency $\eta_f = |\tau_0|$. The profile likelihood in [9, fig. 19, middle] reveals peaks at $\ln\eta_f \in [4.5, 4.8]$ ($|\Delta\chi^2_{\rm bf}| \simeq 2$) and $\ln\eta_f \in [5.3, 5.7]$ ($|\Delta\chi^2_{\rm bf}| \simeq 8$), which is consistent with our results.

It is worth noting that in both searches above the overall best fit occurs at $\ln(-\tau_0) \simeq 8.2\,(|\Delta\chi^2_{\rm bf}| \sim 14)$, too high a frequency for the scope of this work. In [9], and also later in [25, 62], this particular fit has been interpreted as a signal from a step in the inflationary potential. However, in [14, 30] it is argued that the best-fit values of the feature parameters lie outside the allowed theoretical bounds, making its interpretation as a step in the potential inconsistent.

2.5 Comparison with the search for features in Planck's bispectrum

Now that we have put the reliability of our results to the test, we are in a good place to make predictions on the kind of features we expect to see in the bispectrum of the next data release of Planck, if any. They are simply those given by eq. (1.55) evaluated within the c.l. intervals in table 2.1, with relative probabilities to be found given by the best fit likelihood values of each mode. As an example, the bispectrum corresponding to the best fit of mode $\mathcal{B}$ can be seen in fig. 2.8). While we wait for the next data release of the Planck survey, we can try to assess the fulfilment of this predictions based on the preliminary results for the bispectrum published in the Planck data release of March 2013 [10].

A search for linearly oscillatory features was performed in Planck's bispectrum (cf. [10, sec. 7.3.3]), using as a template [32]

$$B(k_1,k_2,k_3) = \frac{6A^2 f_{\rm NL}^{\rm feat}}{(k_1k_2k_3)^2}\sin\left(2\pi\frac{\sum_{i=1}^3 k_i}{3k_c}+\phi\right)\,, \tag{2.8}$$

where $A = A_s k_*^{1-n_s}$, A_s and n_s being the amplitude and spectral index of the primordial power spectrum, and $k_* = 0.05\,{\rm Mpc}^{-1}$ a pivot scale. They sampled the amplitude $f_{\rm NL}^{\rm feat}$ over a coarse grid of wavelengths k_c and phases ϕ.

Our features also present a linearly oscillatory pattern, which comes from the Fourier transform in (1.54). These oscillations enter the bispectrum approximately as $\exp(i\sum_i k_i\tau_0)$, cf. eq. (1.55) and (1.54), which compares to Planck's search as $\tau_0 \approx 2\pi/(3k_c)$. Thus, Planck's search falls inside $\ln(-\tau_0) \in [4.43, 5.34]$, while ours spans up to $\ln(-\tau_0) = 6$ $\left(k_c = 0.00519\,{\rm Mpc}^{-1}\right)$. The overlap includes our modes $\mathcal{C}$ and $\mathcal{D}$ (and also the discarded $\mathcal{E}$). For every combination of the feature parameter values in the regions of high likelihood, one can find a combination of the parameters in [10] (including a gaussian envelope as described there) such that the correlation between both shapes at the primordial level is al least 95%.

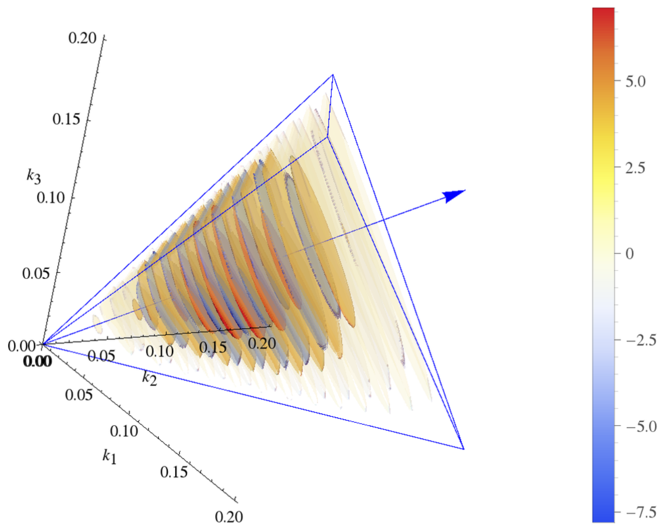

(a) Full 3D primordial bispectrum (in colour in the the on-line version of [1]

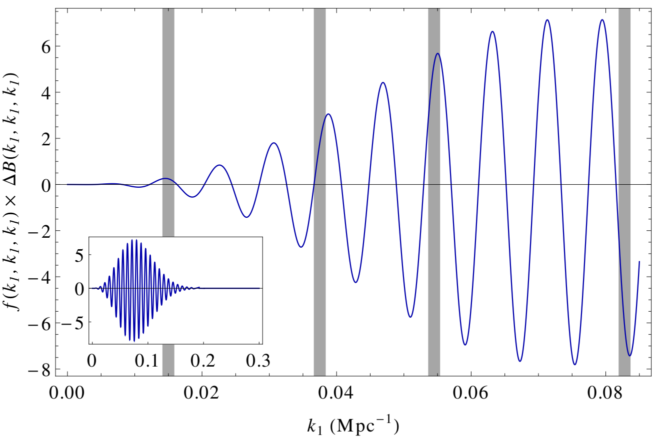

(b) Equilateral limit. The grey stripes show the approximate scales of the first four acoustic peaks in the CMB power spectrum, and a zoom-out is shown at the lower-left corner. Most of the signal at high k, i.e. small scales, would be suppressed by diffusion damping when transferred to the CMB.

Figure 2.8: Prediction for the *primordial* bispectrum for the best fit of mode $\mathcal{B}$, normalized by $f(k_1, k_2, k_3) = (10/3)\,[(2\pi)^2 A_s k_*^{1-n_s}]^{-2} \prod_i k_i^3 \,/\, \sum_i k_i^3$.

The search in [10] is later supplemented with a gaussian envelope centred at scales corresponding to the first acoustic peak, which dampens the signal in subsequent peaks for decreasing values of a falloff Δk.[5] The envelope generally improves the significance, except for the 2σ signal at $k_c = 0.01375\,,0.01500\,\mathrm{Mpc}^{-1}$. This suggests that this band's significance comes mostly from the second and third peaks (the signal from the fourth on would be most likely damped out).

In comparison, our best fits to the power spectrum predict bispectrum features which are mild at the first peak and more intense from the second peak onwards. The higher the value of $\ln\beta$, the smaller the scale at which the feature peaks. In the range of $\ln(-\tau_0)$ probed here, we were not able to reproduce the improvement Planck appears to see for features at the first peak. On the other hand, we find good matching around the second and third peak scales between the best fit of $\mathcal{D}$ with $k_c = 0.01327\,\mathrm{Mpc}^{-1}$ and the 2.3σ signal of Planck at $k_c = 0.01375\,\mathrm{Mpc}^{-1}$ with $f_{\mathrm{NL}}^{\mathrm{feat}} = 345$ and $\phi = \pi/2$ (see fig. 2.9). A similar but milder qualitative matching also occurs on the same scales between the best fit of $\mathcal{C}$ with $k_c = 0.01014\,\mathrm{Mpc}^{-1}$ and Planck's 2.6σ signal with $k_c = 0.01125\,\mathrm{Mpc}^{-1}$. Although these matchings are not easy to quantify at the moment of writing this thesis, they suggest enlarging the search in [10] to test envelopes centred at smaller scales, and also to cover the frequencies corresponding to modes $\mathcal{A}$ and $\mathcal{B}$.

Note that we have quoted the fits to the Bispectrum of Planck without applying the *look-elsewhere effect*. This effect will be properly taken into account when a full study of the Bayesian evidence is performed in a future work, and it is expected to reduce the significance in a much smaller amount [39] than that quoted in [10], since the signals in both data sets, spectrum and bispectrum, are sampled over a single parameter space.

2.6 Conclusions and discussion

We have carried out a statistical search for localized oscillatory features in the CMB power spectrum produced by a transient reduction in the speed of sound. We have found a number of fits and we have performed additional tests to the results. Namely, we have tried to replicate them using independent codes and found practically equal results; we have studied more explicitly the small degeneracies among the cosmological and feature parameters, and proposed the CMB TE and EE polarization spectra as a way to break degeneracies among the latter; and finally we have investigated at which multipoles each of our fits describe the CMB temperature data better than the baseline ΛCDM model.

For each of the modes, we have calculated the associated primordial bispectra. Because of the small amplitude at the best fits, the bispectrum prediction closely resembles that of step inflation, tested by the Planck collaboration, since a transient slow-roll violation switches on the same operator in the cubic action. It is then straightforward to compare our prediction with the templates used in that

[5] James Fergusson, private communication.

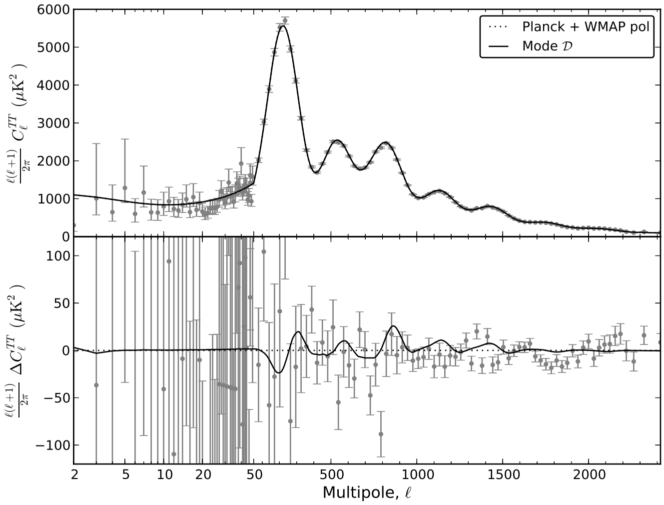

(a) Comparison of Planck's CMB power spectrum (dotted) and the corresponding best fit of the mode $\mathcal{D}$ (solid).

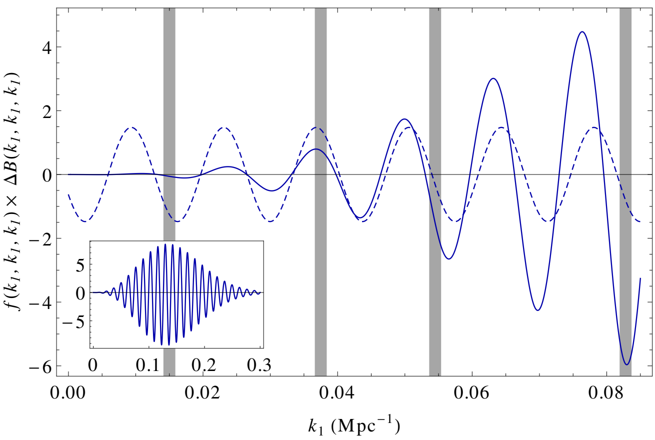

(b) Comparison along the equilateral direction of Planck's 2.3σ *primordial* bispectrum fit with $k_c = 0.01375\,\mathrm{Mpc}^{-1}$ (dashed), and the expected signal in the *primordial* bispectrum for the best fit of $\mathcal{D}$ (solid). Both bispectra are normalized by $f(k_1, k_2, k_3) = (10/3)\left((2\pi)^2 A_s k_*^{1-n_s}\right)^{-2} \prod_i k_i^3 \,/\, \sum_i k_i^3$. The grey stripes show the approximate scales corresponding to the first four acoustic peaks in the CMB power spectrum. Although our signal extends beyond those scales (see zoom-out at the lower-left corner), from the third peak on, the primordial signal is highly suppressed by diffusion damping when transferred to the CMB.

Figure 2.9: Features corresponding to the best fit of the mode $\mathcal{D}$ (see table 2.1), for which the comparison with Planck analysis for the bispectrum is possible.

search, and the agreement is surprisingly good. This is remarkable, considering that these bispectrum features are *predicted from a search in the CMB power spectrum* with a very simple *ansatz* for c_s.

The functional form chosen for the reduction in the speed of sound is inspired by soft turns in a multi-field inflationary trajectory with a large hierarchy of masses, a situation that is consistent with an effectively single-field description with uninterrupted slow-roll. Other functional forms and parameter ranges are under investigation. We stress that our analysis is independent of the physical mechanism behind the reduction.

We emphasize that the CMB power spectrum data alone can hardly justify the introduction of features on top of the ΛCDM model; a gain of $|\Delta\chi^2| \lesssim 10$ is not uncommon. However, as we have shown, low-significance fits in the power spectrum can still predict correlated features that may be observable in the CMB bispectrum. Therefore, model selection should take into account both observables simultaneously.

The ability to make predictions in a wider region of the parameter space of features is of particular relevance, since new data sets may allow us to explore it. Besides, since different experiments generally have different foregrounds and systematics, a joint analysis could reduce the contamination of the primordial signal on the overlapping scales. In particular, we later extended our search to large scale structure surveys, see [49] or chapter 3.

Our results suggest that, by exploiting correlations between different observables, current data might already be sensitive enough to detect transient reductions in the speed of sound as mild as a few percent, opening a new window for the presence of extra degrees of freedom during inflation.

Bibliography

[1] Ana Achucarro, Vicente Atal, Pablo Ortiz, and Jesus Torrado. Localized correlated features in the CMB power spectrum and primordial bispectrum from a transient reduction in the speed of sound. *Phys.Rev.*, D89:103006, 2014, 1311.2552.

[2] Ana Achucarro, Jinn-Ouk Gong, Sjoerd Hardeman, Gonzalo A. Palma, and Subodh P. Patil. Features of heavy physics in the CMB power spectrum. *JCAP*, 1101:030, 2011, 1010.3693.

[3] Ana Achucarro, Jinn-Ouk Gong, Sjoerd Hardeman, Gonzalo A. Palma, and Subodh P. Patil. Mass hierarchies and non-decoupling in multi-scalar field dynamics. *Phys.Rev.*, D84:043502, 2011, 1005.3848.

[4] Ana Achucarro, Jinn-Ouk Gong, Sjoerd Hardeman, Gonzalo A. Palma, and Subodh P. Patil. Effective theories of single field inflation when heavy fields matter. *JHEP*, 1205:066, 2012, 1201.6342.

[5] Ana Achucarro, Jinn-Ouk Gong, Gonzalo A. Palma, and Subodh P. Patil. Correlating features in the primordial spectra. *Phys.Rev.*, D87:121301, 2013, 1211.5619.

[6] Jennifer A. Adams, Bevan Cresswell, and Richard Easther. Inflationary perturbations from a potential with a step. *Phys.Rev.*, D64:123514, 2001, astro-ph/0102236.

[7] P.A.R. Ade et al. Planck 2013 results. I. Overview of products and scientific results. 2013, 1303.5062.

[8] P.A.R. Ade et al. Planck 2013 results. XV. CMB power spectra and likelihood. 2013, 1303.5075.

[9] P.A.R. Ade et al. Planck 2013 results. XXII. Constraints on inflation. 2013, 1303.5082.

[10] P.A.R. Ade et al. Planck 2013 Results. XXIV. Constraints on primordial non-Gaussianity. 2013, 1303.5084.

[11] P.A.R. Ade et al. Planck 2013 results. XVI. Cosmological parameters. *Astron.Astrophys.*, 2014, 1303.5076.

[12] Peter Adshead, Cora Dvorkin, Wayne Hu, and Eugene A. Lim. Non-Gaussianity from Step Features in the Inflationary Potential. *Phys.Rev.*, D85:023531, 2012, 1110.3050.

[13] Peter Adshead and Wayne Hu. Fast Computation of First-Order Feature-Bispectrum Corrections. *Phys.Rev.*, D85:103531, 2012, 1203.0012.

[14] Peter Adshead and Wayne Hu. Bounds on non-adiabatic evolution in single-field inflation. *Phys.Rev.*, D89:083531, 2014, 1402.1677.

[15] Peter Adshead, Wayne Hu, Cora Dvorkin, and Hiranya V. Peiris. Fast Computation of Bispectrum Features with Generalized Slow Roll. *Phys.Rev.*, D84:043519, 2011, 1102.3435.

[16] Peter Adshead, Wayne Hu, and Vin?cius Miranda. Bispectrum in Single-Field Inflation Beyond Slow-Roll. *Phys.Rev.*, D88:023507, 2013, 1303.7004.

[17] Moumita Aich, Dhiraj Kumar Hazra, L. Sriramkumar, and Tarun Souradeep. Oscillations in the inflaton potential: Complete numerical treatment and comparison with the recent and forthcoming CMB datasets. *Phys.Rev.*, D87:083526, 2013, 1106.2798.

[18] Andreas Albrecht and Paul J. Steinhardt. Cosmology for Grand Unified Theories with Radiatively Induced Symmetry Breaking. *Phys.Rev.Lett.*, 48:1220–1223, 1982.

[19] Frederico Arroja, Antonio Enea Romano, and Misao Sasaki. Large and strong scale dependent bispectrum in single field inflation from a sharp feature in the mass. *Phys.Rev.*, D84:123503, 2011, 1106.5384.

[20] Frederico Arroja and Misao Sasaki. Strong scale dependent bispectrum in the Starobinsky model of inflation. *JCAP*, 1208:012, 2012, 1204.6489.

[21] Amjad Ashoorioon and Axel Krause. Power Spectrum and Signatures for Cascade Inflation. 2006, hep-th/0607001.

[22] Benjamin Audren, Julien Lesgourgues, Karim Benabed, and Simon Prunet. Conservative Constraints on Early Cosmology: an illustration of the Monte Python cosmological parameter inference code. *JCAP*, 1302:001, 2013, 1210.7183.

[23] Nicola Bartolo, Dario Cannone, and Sabino Matarrese. The Effective Field Theory of Inflation Models with Sharp Features. *JCAP*, 1310:038, 2013, 1307.3483.

[24] Rachel Bean, Xingang Chen, Girma Hailu, S.-H. Henry Tye, and Jiajun Xu. Duality Cascade in Brane Inflation. *JCAP*, 0803:026, 2008, 0802.0491.

[25] M. Benetti. Updating constraints on inflationary features in the primordial power spectrum with the Planck data. *Phys.Rev.*, D88(8):087302, October 2013, 1308.6406.

[26] Micol Benetti, Massimiliano Lattanzi, Erminia Calabrese, and Alessandro Melchiorri. Features in the primordial spectrum: new constraints from WMAP7+ACT data and prospects for Planck. *Phys.Rev.*, D84:063509, 2011, 1107.4992.

[27] Micol Benetti, Stefania Pandolfi, Massimiliano Lattanzi, Matteo Martinelli, and Alessandro Melchiorri. Featuring the primordial power spectrum: new constraints on interrupted slow-roll from CMB and LRG data. *Phys.Rev.*, D87:023519, 2013, 1210.3562.

[28] C.L. Bennett et al. Nine-Year Wilkinson Microwave Anisotropy Probe (WMAP) Observations: Final Maps and Results. *Astrophys.J.Suppl.*, 208:20, 2013, 1212.5225.

[29] Diego Blas, Julien Lesgourgues, and Thomas Tram. The Cosmic Linear Anisotropy Solving System (CLASS) II: Approximation schemes. *JCAP*, 1107:034, 2011, 1104.2933.

[30] Dario Cannone, Nicola Bartolo, and Sabino Matarrese. Perturbative Unitarity of Inflationary Models with Features. *Phys.Rev.*, D89:127301, 2014, 1402.2258.

[31] Sebastian Cespedes, Vicente Atal, and Gonzalo A. Palma. On the importance of heavy fields during inflation. *JCAP*, 1205:008, 2012, 1201.4848.

[32] Xingang Chen, Richard Easther, and Eugene A. Lim. Large Non-Gaussianities in Single Field Inflation. *JCAP*, 0706:023, 2007, astro-ph/0611645.

[33] Xingang Chen, Richard Easther, and Eugene A. Lim. Generation and Characterization of Large Non-Gaussianities in Single Field Inflation. *JCAP*, 0804:010, 2008, 0801.3295.

[34] Clifford Cheung, Paolo Creminelli, A. Liam Fitzpatrick, Jared Kaplan, and Leonardo Senatore. The Effective Field Theory of Inflation. *JHEP*, 0803:014, 2008, 0709.0293.

[35] Jeongyeol Choe, Jinn-Ouk Gong, and Ewan D. Stewart. Second order general slow-roll power spectrum. *JCAP*, 0407:012, 2004, hep-ph/0405155.

[36] Laura Covi, Jan Hamann, Alessandro Melchiorri, Anze Slosar, and Irene Sorbera. Inflation and WMAP three year data: Features have a Future! *Phys.Rev.*, D74:083509, 2006, astro-ph/0606452.

[37] Ulf H. Danielsson. A Note on inflation and transPlanckian physics. *Phys.Rev.*, D66:023511, 2002, hep-th/0203198.

[38] Cora Dvorkin and Wayne Hu. Generalized Slow Roll for Large Power Spectrum Features. *Phys.Rev.*, D81:023518, 2010, 0910.2237.

[39] J.R. Fergusson, H.F. Gruetjen, E.P.S. Shellard, and M. Liguori. Combining power spectrum and bispectrum measurements to detect oscillatory features. 2014, 1410.5114.

[40] F. Feroz, M.P. Hobson, and M. Bridges. MultiNest: an efficient and robust Bayesian inference tool for cosmology and particle physics. *Mon.Not.Roy.Astron.Soc.*, 398:1601–1614, 2009, 0809.3437.

[41] Farhan Feroz and M.P. Hobson. Multimodal nested sampling: an efficient and robust alternative to MCMC methods for astronomical data analysis. *Mon.Not.Roy.Astron.Soc.*, 384:449, 2008, 0704.3704.

[42] Raphael Flauger, Liam McAllister, Enrico Pajer, Alexander Westphal, and Gang Xu. Oscillations in the CMB from Axion Monodromy Inflation. *JCAP*, 1006:009, 2010, 0907.2916.

[43] X. Gao, D. Langlois, and S. Mizuno. Oscillatory features in the curvature power spectrum after a sudden turn of the inflationary trajectory. *JCAP*, 10:23, 2013, 1306.5680.

[44] Xian Gao, David Langlois, and Shuntaro Mizuno. Influence of heavy modes on perturbations in multiple field inflation. *JCAP*, 1210:040, 2012, 1205.5275.

[45] Jinn-Ouk Gong. Breaking scale invariance from a singular inflaton potential. *JCAP*, 0507:015, 2005, astro-ph/0504383.

[46] Brian R. Greene, Koenraad Schalm, Gary Shiu, and Jan Pieter van der Schaar. Decoupling in an expanding universe: Backreaction barely constrains short distance effects in the CMB. *JCAP*, 0502:001, 2005, hep-th/0411217.

[47] Alan H. Guth. The Inflationary Universe: A Possible Solution to the Horizon and Flatness Problems. *Phys.Rev.*, D23:347–356, 1981.

[48] Jan Hamann, Laura Covi, Alessandro Melchiorri, and Anze Slosar. New Constraints on Oscillations in the Primordial Spectrum of Inflationary Perturbations. *Phys.Rev.*, D76:023503, 2007, astro-ph/0701380.

[49] Bin Hu and Jesús Torrado. Searching for primordial localized features with CMB and LSS spectra. 2014, 1410.4804.

[50] Wayne Hu. Generalized Slow Roll for Non-Canonical Kinetic Terms. *Phys.Rev.*, D84:027303, 2011, 1104.4500.

[51] Mark G. Jackson and Koenraad Schalm. Model Independent Signatures of New Physics in the Inflationary Power Spectrum. *Phys.Rev.Lett.*, 108:111301, 2012, 1007.0185.

[52] Julien Lesgourgues. The Cosmic Linear Anisotropy Solving System (CLASS) I: Overview. 2011, 1104.2932.

[53] Antony Lewis and Sarah Bridle. Cosmological parameters from CMB and other data: a Monte- Carlo approach. *Phys. Rev.*, D66:103511, 2002, astro-ph/0205436.

[54] Antony Lewis, Anthony Challinor, and Anthony Lasenby. Efficient computation of CMB anisotropies in closed FRW models. *Astrophys.J.*, 538:473–476, 2000, astro-ph/9911177.

[55] Andrei D. Linde. A New Inflationary Universe Scenario: A Possible Solution of the Horizon, Flatness, Homogeneity, Isotropy and Primordial Monopole Problems. *Phys.Lett.*, B108:389–393, 1982.

[56] Jerome Martin and Christophe Ringeval. Superimposed oscillations in the WMAP data? *Phys.Rev.*, D69:083515, 2004, astro-ph/0310382.

[57] Jerome Martin and L. Sriramkumar. The scalar bi-spectrum in the Starobinsky model: The equilateral case. *JCAP*, 1201:008, 2012, 1109.5838.

[58] P. D. Meerburg, R. A. M. J. Wijers, and J. P. van der Schaar. WMAP7 constraints on oscillations in the primordial power spectrum. *MNRS*, 421:369–380, March 2012, 1109.5264.

[59] P. Daniel Meerburg and David N. Spergel. Searching for Oscillations in the Primordial Power Spectrum: Constraints from Planck (Paper II). *Phys.Rev.*, D89:063537, 2014, 1308.3705.

[60] P. Daniel Meerburg, David N. Spergel, and Benjamin D. Wandelt. Searching for Oscillations in the Primordial Power Spectrum: Perturbative Approach (Paper I). *Phys.Rev.*, D89:063536, 2014, 1308.3704.

[61] Pieter Daniel Meerburg, Jan Pieter van der Schaar, and Pier Stefano Corasaniti. Signatures of Initial State Modifications on Bispectrum Statistics. *JCAP*, 0905:018, 2009, 0901.4044.

[62] Vinicius Miranda and Wayne Hu. Inflationary Steps in the Planck Data. *Phys.Rev.*, D89:083529, 2014, 1312.0946.

[63] Vinicius Miranda, Wayne Hu, and Peter Adshead. Warp Features in DBI Inflation. *Phys.Rev.*, D86:063529, 2012, 1207.2186.

[64] Masahiro Nakashima, Ryo Saito, Yu-ichi Takamizu, and Jun'ichi Yokoyama. The effect of varying sound velocity on primordial curvature perturbations. *Prog.Theor.Phys.*, 125:1035–1052, 2011, 1009.4394.

[65] Toshifumi Noumi and Masahide Yamaguchi. Primordial spectra from sudden turning trajectory. *JCAP*, 1312:038, 2013, 1307.7110.

[66] Minjoon Park and Lorenzo Sorbo. Sudden variations in the speed of sound during inflation: features in the power spectrum and bispectrum. *Phys.Rev.*, D85:083520, 2012, 1201.2903.

[67] Hiranya Peiris, Richard Easther, and Raphael Flauger. Constraining Monodromy Inflation. *JCAP*, 1309:018, 2013, 1303.2616.

[68] Raquel H. Ribeiro. Inflationary signatures of single-field models beyond slow-roll. *JCAP*, 1205:037, 2012, 1202.4453.

[69] Ryo Saito and Yu-ichi Takamizu. Localized Features in Non-Gaussianity from Heavy Physics. *JCAP*, 1306:031, 2013, 1303.3839.

[70] K. Sato. First Order Phase Transition of a Vacuum and Expansion of the Universe. *Mon.Not.Roy.Astron.Soc.*, 195:467–479, 1981.

[71] Alexei A. Starobinsky. Relict Gravitation Radiation Spectrum and Initial State of the Universe. (In Russian). *JETP Lett.*, 30:682–685, 1979.

[72] Alexei A. Starobinsky. Dynamics of Phase Transition in the New Inflationary Universe Scenario and Generation of Perturbations. *Phys.Lett.*, B117:175–178, 1982.

[73] Alexei A. Starobinsky. Spectrum of adiabatic perturbations in the universe when there are singularities in the inflation potential. *JETP Lett.*, 55:489–494, 1992.

[74] Ewan D. Stewart. The Spectrum of density perturbations produced during inflation to leading order in a general slow roll approximation. *Phys.Rev.*, D65:103508, 2002, astro-ph/0110322.

[75] Yu-ichi Takamizu, Shinji Mukohyama, Misao Sasaki, and Yoshiharu Tanaka. Non-Gaussianity of superhorizon curvature perturbations beyond δ N formalism. *JCAP*, 1006:019, 2010, 1004.1870.

[76] Licia Verde. Statistical methods in cosmology. *Lect.Notes Phys.*, 800:147–177, 2010, 0911.3105.

[77] Li-Min Wang and Marc Kamionkowski. The Cosmic microwave background bispectrum and inflation. *Phys.Rev.*, D61:063504, 2000, astro-ph/9907431.